CHEMISTRY
A EUROPEAN JOURNAL

DOI: 10.1002/chem.200800294

Similar Biological Activities of Two Isostructural Ruthenium and Osmium Complexes

Jasna Maksimoska,[a] Douglas S. Williams,[a] G. Ekin Atilla-Gokcumen,[b] Keiran S. M. Smalley,[c] Patrick J. Carroll,[a] Richard D. Webster,[d] Panagis Filippakopoulos,[e] Stefan Knapp,[e] Meenhard Herlyn,[c] and Eric Meggers*[b]

Abstract: In this study, we probe and verify the concept of designing unreactive bioactive metal complexes, in which the metal possesses a purely structural function, by investigating the consequences of replacing ruthenium in a bioactive half-sandwich kinase inhibitor scaffold by its heavier congener osmium. The two isostructural complexes are compared with respect to their anticancer properties in 1205 Lu melanoma cells, activation of the Wnt signaling pathway, IC_{50} values against the protein kinases GSK-3β and Pim-1, and binding modes to the protein kinase Pim-1 by protein crystallography. It was found that the two congeners display almost indistinguishable biological activities, which can be explained by their nearly identical three-dimensional structures and their identical mode of action as protein kinase inhibitors. This is a unique example in which the replacement of a metal in an anticancer scaffold by its heavier homologue does not alter its biological activity.

Keywords: antitumor agents · bioorganometallic chemistry · kinase inhibitors · osmium · ruthenium

Introduction

Metal complexes offer vast opportunities for the design of compounds with bioactivity due to the large variety of available metals and the ability to tune the reactivity and structure of the metal complexes by their ligand spheres.[1] Most commonly, the metal is directly involved in the mode of action, either through coordination or redox chemistry. For example, the highly successful anticancer drug cisplatin (**1**)

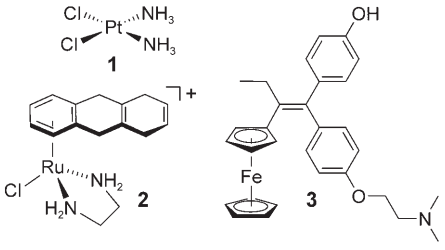

crosslinks guanine bases in DNA duplexes.[2] Similarly, the ruthenium arene complex **2** and its derivatives exert their highly cytotoxic effects through coordination to DNA,[3] whereas the ferrocene moiety in the breast cancer drug candidate hydroxyferrocifen (**3**) is believed to serve as a crucial redox-active moiety.[4] Thus, these reactive anticancer drugs require a fine-tuned reactivity of the metal center, and it is, therefore, not surprising that in these complexes a substitution of the metal by one of their homologues results in a decline in anticancer activities: the palladium analogue of cis-

[a] J. Maksimoska, D. S. Williams, Dr. P. J. Carroll
Department of Chemistry, University of Pennsylvania
231 South 34th Street, Philadelphia
PA 19104 (USA)

[b] G. E. Atilla-Gokcumen, Prof. Dr. E. Meggers
Fachbereich Chemie, Philipps-Universität Marburg
Hans-Meerwein-Strasse
35043 Marburg (Germany)
Fax: (+49) 6421-282-2189
E-mail: meggers@chemie.uni-marburg.de

[c] Dr. K. S. M. Smalley, Prof. M. Herlyn
The Wistar Institute, 3601 Spruce Street
Philadelphia, PA 19104 (USA)

[d] Prof. R. D. Webster
Division of Chemistry and Biological Chemistry
Nanyang Technological University
637616 (Singapore)

[e] Dr. P. Filippakopoulos, Dr. S. Knapp
Centre for Structural Genomics
Botnar Research Centre, Oxford University
Oxford OX3 7LD (UK)

Supporting information for this article is available on the WWW under http://www.chemeurj.org/ or from the author and contains crystallographic data for **OsBn** and cell cycle analysis data.

platin is too hydrolytically unstable to serve as an anticancer drug, but the osmium analogue of **2** hydrolyzes by two orders of magnitude more slowly than the ruthenium congener and, therefore, should react more slowly with DNA;[5] the ruthenium analogue of hydroxyferrocifen **3**, unlike the ferrocifens, does not show antiproliferate effects on estrogen receptor α-negative breast cancer cell lines, most likely due to a modified redox behavior.[6]

We recently revealed the promising kinase inhibition and anticancer effects of the ruthenium half-sandwich complex **Ru** and some of its derivatives (Scheme 1).[7–12] The organometallic **Ru** is a highly potent inhibitor for the kinases GSK-3, Pim-1,[8,10,11] and probably some yet unidentified kinases, and induces strong biological responses, such as the activation of the Wnt signaling pathway in mammalian cells,[8] strong pharmacological effects during the development of frog embryos,[8] and the efficient induction of apoptosis in some melanoma cell lines.[12] In contrast to the aforementioned examples **1**–**3**, we believe that the ruthenium center in the scaffold **Ru** has a solely structural role, and that it is rather the shape of the organometallic complex that is responsible for all of its bioactivity.[10]

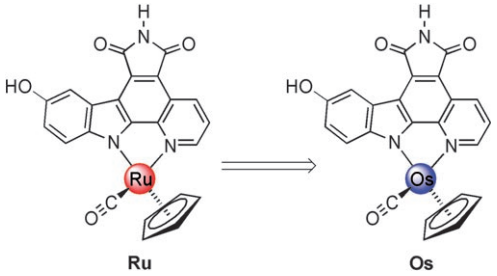

Scheme 1. Probing the correlation between shape and function with the isostructural complexes **Ru** and **Os**.

We sought to probe this assumption by replacing ruthenium by its heavier homologue, osmium (**Ru**→**Os**, Scheme 1).[5,13] Ruthenium and osmium, which are located within the same group in the second and third transition-metal row, respectively, form isostructural complexes because the atomic radii of the two elements are almost identical due to the lanthanide contraction.[14] Despite these structural similarities, third-row transition-metal ions are generally significantly more substitutionally inert than those of the second row, and possess a different redox chemistry.[15] Therefore, if the reactivity of the metal plays at least some role in the mode of action, **Ru** and **Os** should differ significantly in their bioactivities. In contrast, if indeed the three-dimensional structures of these organometallic scaffolds determine their bioactivities, the two congeners **Ru** and **Os** must display closely related properties. The following study demonstrates that the latter is indeed the case: **Ru** and **Os** display almost indistinguishable biological activities, thus verifying the concept of designing unreactive bioactive metal complexes with the metal serving as a key structural center.

Results and Discussion

Synthesis of osmium half-sandwich complexes: Compound **Os** was obtained in an analogous fashion to the recently described synthesis of **Ru** (Scheme 2).[16] Accordingly, the pyridocarbazole ligand **4** was reacted with $[Os(\eta^5\text{-}C_5H_5)(CO)(MeCN)_2]^+PF_6^-$ (**5**)[17] in the presence of one equivalent of potassium carbonate, followed by a tetrabutylammonium fluoride (TBAF)-induced desilylation, to afford **Os** in a modest yield of 31% over two steps. This synthetic scheme is general and applicable to derivatives of **Os**, such as **OsBn**, in which a benzyl group at the imide moiety serves as a crystallization handle (see Figure 1).

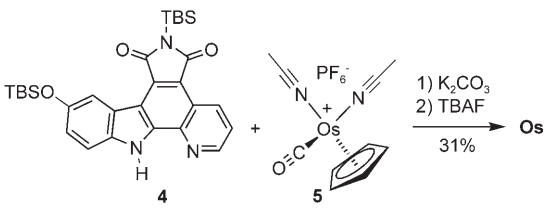

Scheme 2. Synthesis of **Os**. TBAF = tetra-*n*-butylammonium fluoride; TBS = *tert*-butyldimethylsilyl.

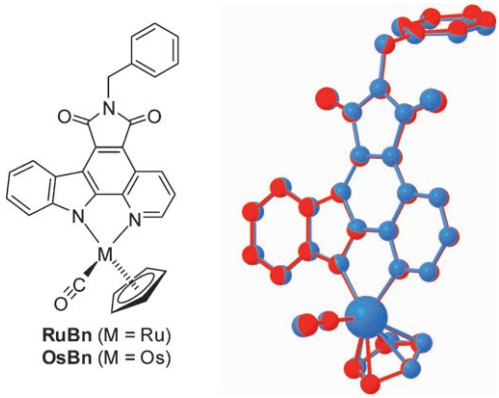

Figure 1. Superimposed crystal structures of **RuBn** (red) and **OsBn** (blue).

Structural comparison of ruthenium and osmium complexes: To evaluate the structural similarity of **Ru** and **Os**, we crystallized the derivative **OsBn** and compared the obtained crystal structure with the analogous and recently described ruthenium crystal structure **RuBn**.[7] A superimposition revealed that both complexes are almost indistinguishable in their three-dimensional structures (Figure 1). For example, the differences in the coordinative bond length to the CO ($\Delta = 0.004$ Å), the pyridine nitrogen ($\Delta = 0.008$ Å), and the indole nitrogen ($\Delta = 0.004$ Å) are within three times the estimated standard deviations ($3 \times \sigma$) and, therefore, are identical within experimental errors. The discrepancies to the

carbon atoms of the cyclopentadienyl ligand range from 0.001 to 0.032 Å and from less than $1\times\sigma$ to $7\times\sigma$. Altogether, it can be concluded that replacing ruthenium for osmium in this half-sandwich scaffold leads to almost indistinguishable structures.

Configurational stabilities and redox potentials: Despite this desired structural conformity, osmium typically forms coordinative bonds that are more inert than the analogous bonds of its lighter homologue, ruthenium.[15] In our scaffold, this phenomenon is reflected by the significantly higher configurational stability of **Os** compared to **Ru**. To evaluate this, a sample of (*R*)-**Os** (10 mM in DMSO) was stored in the dark at room temperature for one month and then analyzed with a Daicel Chiralpak 1B HPLC column (45:55→80:20 EtOH/hexane in 20 minutes, flow rate = 0.5 mL min^{-1}), after which no trace of the mirror image (*S*)-**Os** could be observed. In contrast, the enantiopure ruthenium complexes racemize at room temperature by about 3% in one week; this reflects the higher inertness of the **Os** complex compared to the **Ru** complex. With respect to redox behavior, **Ru** and **Os** differ only slightly: the oxidative peak potential of **Os** (E_p^{ox} = 0.312 V vs. Fc/Fc$^+$ (Fc$^+$ = ferrocene/ium)) is around 50 mV lower than **Ru** (E_p^{ox} = 0.36 V vs. Fc/Fc$^+$).

Anticancer activities in 1205 Lu melanoma cells: We initiated our comparative bioactivity study by measuring the cytotoxicities of **Ru** and **Os** in melanoma cells.[12] For this, we incubated 1205 Lu cells with different concentrations of the organometallic compounds (3 nM to 3 μM) for 72 h and quantified the reduction of live cells with the MTT method. The results in Figure 2a demonstrate that within experimental errors, **Ru** and **Os** show almost identical concentration-dependent cytotoxicity profiles in 1205 Lu. For example, at 1 μM, the cell survival is at (16 ± 4)% and (18 ± 7)% for **Ru** and **Os**, respectively.

To investigate this further in a more complex model, **Ru** and **Os** were tested in collagen-implanted three-dimensional spheroids of 1205 Lu cells.[12] As shown in Figure 2b, at concentrations as low as 3 μM, both compounds decreased cell viability markedly and to a similar extent, as visualized by the loss of green fluorescent live cells and the appearance of red fluorescent dead cells.[12] Thus, **Ru** and **Os** display highly potent and almost identical antiproliferate properties. Furthermore, cell cycle analyses of 1205 Lu cells that were treated with **Ru** and **Os** for 24 h, revealed a concentration-dependent increase in the number of cells in the sub-G1 population, which indicates that the induction of apoptosis was the main reason for cell death. Levels of apoptosis were very similar for **Ru** and **Os**, reaching 24 and 27% at 1 μM, and 50 and 41% at 3 μM, respectively (see the Supporting Information).

Activation of Wnt signaling: We recently disclosed that the strong apoptotic effect of complex **Ru** in 1205 Lu cells occurs at least in part through p53-induced apoptosis, which is initiated by the inhibition of glycogen synthase kinase 3β (GSK-3β).[12] Therefore, we next compared **Os** and **Ru** in their ability to inhibit GSK-3β in vitro and within mammalian cells. We first measured IC_{50} values against GSK-3β with an enzyme assay and found that both **Ru** and **Os** show very similar binding behavior, with **Os** the slightly more potent inhibitor for GSK-3β with an IC_{50} of (0.6 ± 0.2) nM versus (1.4 ± 0.4) nM for **Ru** at 100 μM ATP (Figure 3a).[18] GSK-3β is a negative regulator of the Wnt signal transduction pathway and, therefore, the inhibition of GSK-3β results in the activation of β-catenin-dependent transcription.[19] To compare the activation of Wnt signaling as a response to GSK-3β inhibition inside mammalian cells upon **Ru** and **Os** treatment, we used human embryonic kidney cells (HEK293OT) that are stably transfected with a TCF/β-catenin luciferase

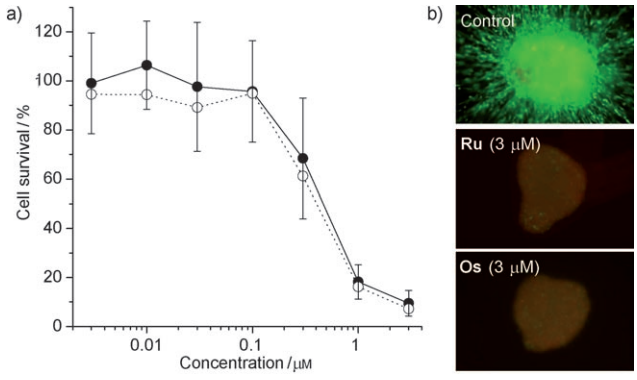

Figure 2. Anticancer properties of **Os** and **Ru**. a) 1205 Lu melanoma cells were treated with **Os** (●) and **Ru** (○) for 72 h and cell survival was determined by using the MTT assay. The average of five independent experiments is shown. b) Collagen-implanted 1205 Lu spheroids were overlaid with the medium and incubated with **Os** and **Ru** for 72 h before treatment with calcein-AM and propidium iodide. Green fluorescence indicates viable cells and red fluorescence dead cells.

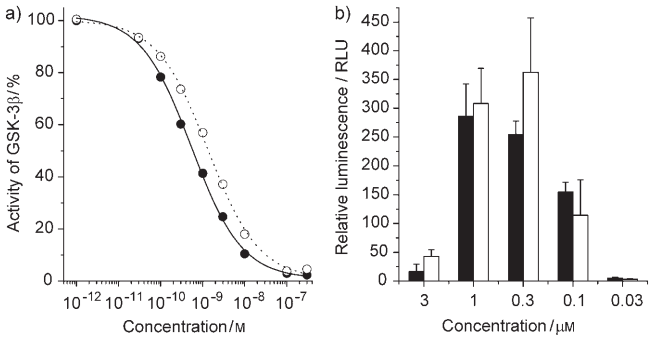

Figure 3. Inhibition of GSK-3β by **Os** and **Ru** in vitro and within mammalian cells. a) GSK-3β inhibition at 100 μM ATP and 200 pM GSK-3β (●: **Os**; ○: **Ru**). IC_{50} curves were obtained by phosphorylation of phospho-glycogen synthase peptide-2 with [γ-^{32}P]ATP. Every data point was determined from at least two independent measurements and the error bars are less than 20%. b) Activation of the Wnt signaling pathway by the inhibition of GSK-3β (■: **Os**; □: **Ru**). HEK293 cells that were transfected with a β-catenin-responsive luciferase reporter were treated with different concentrations of compounds for 24 h. Luminescence signals were measured after cell lysis and the addition of luciferin. The average of four individual experiments is shown.

reporter gene (OT-Luc cells).[20] This system allows the monitoring of β-catenin levels with a luminescent read-out. Accordingly, we incubated OT-Luc cells with different concentrations of **Ru** and **Os** for 24 h and determined luciferase levels from the addition of luciferin to the cell lysate followed by luminescence signal measurements. The results are shown in Figure 3b. Again, **Ru** and **Os** show a highly similar bell-shaped concentration-dependent Wnt activation profile.

Protein kinase binding: Altogether, the presented data imply that the almost identical anticancer properties of **Ru** and **Os** are the result of their highly similar protein kinase inhibition profiles. To support this conclusion, we attempted to compare the binding modes of the two congeners to a protein kinase by using the protein kinase Pim-1 as a model system. Accordingly, we cocrystallized (*S*)-**Os** with full-length human Pim-1, solved the structure to a resolution of 2.35 Å (Table 1), and compared it with the recently obtained

Table 1. Crystallographic data and refinement statistics of (*S*)-**Os** with Pim-1.

Parameters	
space group	$P6_5$
cell dimensions [Å]	$a,b = 98.45$, $c = 80.36$
resolution [Å]	2.35
total observation (unique, redundancy)	212458 (18397, 11.5)
completeness (outer shell) [%]	97.7 (100.0)
R_{merge} (outer shell) [%]	14.9 (78.9)
I/σ (outer shell)	18.1 (3.5)
R_{work} (R_{free}) [%]	16.8 (22.5)
hetero groups	(*S*)-**Os**
rmsd[a] bond length [Å]	0.016
rmsd[a] bond angle [°]	1.447
Ramachandran [%] (allowed/generally allowed/disallowed)	92.8/7.2/0

[a] rmsd = root-mean-square deviation.

structure of (*S*)-**Ru** and Pim-1.[10] To our knowledge, this crystal structure represents the first disclosed structure of an osmium complex that is bound to an enzyme. Upon superimposing the main-chain atoms of both cocrystal structures (rms deviation of 0.24 Å), (*S*)-**Ru** and (*S*)-**Os** occupy almost indistinguishable binding positions within the ATP-binding site. The same van der Waals interactions that (*S*)-**Ru** establishes with Pim-1 are preserved in the structure with (*S*)-**Os**. The pyridocarbazole moiety of (*S*)-**Os** is nicely placed in the hydrophobic pocket that is formed by the residues from the N- and C-terminal domains; the cyclopentadienyl ring stacks against Phe49, whereas the CO group is positioned in close proximity to Gly45 (Figure 4). In the same way as (*S*)-**Ru**, (*S*)-**Os** forms a characteristic hydrogen bond between the maleimide NH-group and the carbonyl oxygen of Glu121, and the indole hydroxyl group is involved in two additional hydrogen bonds (to Lys67 and water-mediated to Glu89). This is in slight variation to the ruthenium structure in which both of these contacts are water mediated. Importantly, the metal centers are not involved in any direct interaction with the kinase active site, and the two crystal structures are consistent with an experimentally verified identical binding affinity of **Ru** and **Os** to Pim-1 (IC_{50} values of 200 pM at 100 μM ATP).

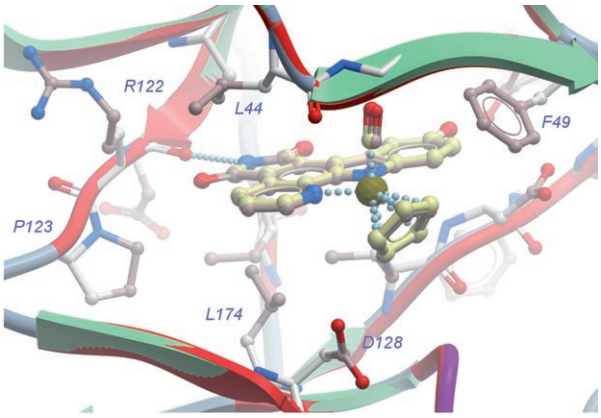

Figure 4. Superimposition of the cocrystal structures of Pim-1 with (*S*)-**Os** (PDB code 3BWF) and (*S*)-**Ru** (PDB code 2BZI). Amino acid side chains are only displayed for the structure with (*S*)-**Os** since the positions are virtually identical. Color coding: Ribbon in red for the ruthenium structure and for the osmium structure green (sheets) and blue (loops). Carbon atoms of (*S*)-**Ru** and (*S*)-**Os** are in pink and yellow, respectively. (*S*)-**Os** is displayed with slightly bigger stick and ball radii to distinguish it from (*S*)-**Ru**.

Conclusion

Swapping ruthenium for the isostructural but chemically distinguished osmium in the organometallic protein kinase inhibitor scaffold (**Ru**→**Os**) enabled us to probe and verify our concept of designing unreactive bioactive metal complexes. To our knowledge, this is a unique example in which the replacement of a metal in an anticancer scaffold by its heavier homologue does not significantly alter the biological activity. This phenomenon can be explained by the almost identical three-dimensional structures of the two complexes and their identical mode of action as protein kinase inhibitors.[21] In fact, an osmium complex with such a high antiproliferative effect in a two- and three-dimensional cell culture is without any precedence. **Ru** and **Os** might thus be members of a new class of bioactive organometallic agents.

Experimental Section

Materials and general methods: NMR spectra were recorded on a Bruker AM-500 (500 MHz) or DMX-360 (360 MHz) spectrometer. IR spectra were recorded on a Perkin–Elmer 1600 series FTIR spectrometer and high-resolution mass spectra were obtained with a Waters LCT Premier instrument by using an ESI ionization and TOF analyzer. Solvents and reagents were used as supplied from Fisher, Sigma–Aldrich, Acros, or Strem. Protein kinases (human) and substrates were purchased from Upstate Biotechnology.

Synthesis of compound Os: A round-bottomed flask was charged with the pyridocarbazole ligand **4**[16a] (50 mg, 0.094 mmol), [Os(η^5-C_5H_5)(CO)-

$(MeCN)_2]^+PF_6^-$ (**5**; 48 mg, 0.094 mmol), [17] K_2CO_3 (13 mg, 0.094 mmol), and a magnetic stir bar. The flask was purged with argon and MeCN (4 mL) and MeOH (1 mL) were added. The reaction was stirred at room temperature for 2 h, during which time the reaction mixture turned purple. The solvent was removed and the crude material was purified by means of silica-gel chromatography by eluting with hexanes/EtOAc 5:1 to 3:1. This yielded the product as a mixture with unreacted ligand. This mixture (36 mg) was used in the next step without further purification.

The mixture (36 mg) was dissolved in CH_2Cl_2 (3 mL) and purged with argon. TBAF (97 μL of a 1 M solution in THF) was added to this solution, which immediately became black and turbid. The reaction was stirred for 30 min at room temperature. Acetic acid (one drop) was added to quench the reaction, upon which the solution turned purple. The solvent was removed and the crude material was purified by means of silica-gel chromatography by eluting with benzene/acetone 10:1 to 5:1. Compound **Os** was isolated as a purple solid (17 mg, 31% over 2 steps). ^{1}H NMR (500 MHz, [D$_6$]DMSO): $\delta = 11.04$ (s, 1H), 9.41 (d, $J = 4.6$ Hz, 1H), 9.23 (s, 1H), 9.00 (d, $J = 8.2$ Hz, 1H), 8.09 (d, $J = 2.4$ Hz, 1H), 7.65 (dd, $J = 8.3$, 5.2 Hz, 1H), 7.51 (d, $J = 8.7$ Hz, 1H), 7.12 (dd, $J = 8.7$, 2.5 Hz, 1H), 5.72 ppm (s, 5H); ^{13}C NMR (125 MHz, [D$_6$]DMSO): $\delta = 182.2$, 170.6, 170.4, 157.8, 156.8, 151.8, 146.30, 146.27, 133.2, 131.3, 123.23, 123.20, 121.1, 116.5, 116.4, 114.5, 112.2, 108.2, 78.2 ppm; IR (thin film): $\tilde{\nu} = 3392$ (br), 2921, 2850, 1916, 1747, 1689, 1643, 1504, 1470, 1339, 1212, 668 cm^{-1}; HRMS: m/z: calcd for $C_{30}H_{20}N_3O_3Os$: 588.0599; found: 588.0602 $[M+H]^+$.

Cyclic voltammetry of Os and Ru: Voltammetric experiments were conducted with a computer-controlled Eco Chemie μAutolab III potentiostat with 1 mm diameter planar Pt and glassy carbon (GC) working electrodes, a Pt wire auxiliary electrode, and an Ag wire reference electrode (isolated by a salt bridge containing 0.5 M Bu_4NPF_6 in CH_3CN). Potentials were referenced to the ferrocene/ferrocenium redox couple. The electrochemical cell was thermostated at 293 K by using an Eyela PSL-1000 variable temperature cooling bath. Data were obtained at a scan rate of 1 V s^{-1} in CH_2Cl_2 with 0.25 M Bu_4NPF_6 as the supporting electrolyte. Oxidative peak potentials (E_P^{ox}): **Ru** = +0.36, **Os** = +0.31 V.

Pim-1 expression, purification, and cocrystallization with Os: Pim-1 was expressed and purified with some modifications as described previously.[22] Briefly, expression of the protein in BL21(DE3)pLysS cells was induced with 2 mM IPTG for 5 h at 18 °C. Cells were collected by centrifugation, resuspended in 50 mM HEPES (pH 7.5), 500 mM NaCl, 5% glycerol, and lysed by applying high pressure (French-press). The lysate was purified with a DEAE cellulose column (DE52 Whatmann) and Ni-NTA chromatography (Qiagen). The protein was treated overnight with lambda phosphatase and TEV protease to remove phosphate and His-tag, respectively. Further purification was achieved with a Mono-Q column (Amersham Biosiences), which separated the dephosphorylated and phosphorylated fractions, and an additional Ni-NTA affinity column to ensure separation of Pim-1 from His-tag. Separated dephosphorylated and phosphorylated fractions were concentrated to 5 mg mL^{-1} in crystallography buffer (50 mM HEPES pH 7.5, 250 mM NaCl, 5% glycerol, 10 mM DTT). The osmium complex (*S*)-**Os** was added to the protein from a 10 mM DMSO stock solution to give a final concentration of 1 mM. Crystals of nonphosphorylated Pim-1 with (*S*)-**Os** were grown at 4 °C in 4 μL sitting drops in which the protein solution (2 μL) was mixed with the precipitate stock (2 μL) that contained 0.2 M Li_2SO_4, 100 mM Bis-TrisPropane (pH 7.0), 20% PEG3350, 10% ethylene glycol, and 0.3% DMSO. Crystals were cryoprotected and flash cooled in liquid nitrogen.

Data collection and structure determination: Cryoprotected crystals yielded X-ray diffraction to 2.35 Å on a X12C beam line at the National Synchrotron Light Source (Upton, NY). Data were indexed and merged by using HKL2000.[23] The structure was solved by molecular replacement by using a crystal structure of Pim-1 (PDB code 1YWV) as a search model for rotation and translation functions, which were calculated with the program AmoRe.[24] Iterative cycles of refinement and manual rebuilding of the model were performed by using the program REFMAC5 and O, respectively.[25,26] The structure has been deposited at the RCSB Protein Data Bank under the PDB code 3BWF.

Measurements of protein kinase inhibition: GSK-3β, Pim-1, and substrates were purchased from Upstate Biotechnology USA. For measuring IC_{50} values of **Os** and **Ru** against Pim-1, various concentrations of inhibitors were incubated at room temperature with 80 pM kinase in MOPS (MOPS = 3-morpholinopropane-1-sulfonic acid; 20 mM, pH 7), bovine serum albumin (0.8 μg μL^{-1}), and 5% DMSO (which is a consequence of the DMSO inhibitor stock solution) in the presence of S6 kinase/Rsk2 substrate peptide (50 μM) and ATP (100 μM), which includes [γ-^{32}P]ATP (0.2 μCi μL^{-1}). Reactions were initiated after 20 min by adding $MgCl_2$ to a final concentration of 30 mM in a total reaction volume of 25 μL. The reactions were terminated by spotting 17.5 μL onto a circular P81 phosphocellulose paper (diameter: 2.1 cm, Whatman) followed by washing with 0.75% phosphoric acid (3×) and acetone (1×). The dried P81 papers were transferred to scintillation vials and a scintillation cocktail (5 mL) was added. The counts per minute (CPM) were measured with a Beckmann 6000 scintillation counter and the IC_{50} values were defined as the concentration of inhibitor at which the CPM was 50% of the control sample corrected by the background.

For determining the IC_{50} values of **Os** and **Ru** against GSK-3β, various concentrations of the compounds were incubated with 200 pM kinase in MOPS (20 mM, pH 7), $MgCl_2$ (30 mM), EDTA (1 mM), bovine serum albumin (0.8 μg μL^{-1}), and 5% DMSO, in the presence of phosphoglycogen synthase kinase-2 substrate (20 μM) for 20 min, and the reactions were initiated by adding ATP to give a final concentration of 100 μM and by including [γ-^{32}P]ATP (0.2 μCi μL^{-1}) to give a final volume of 25 μL. Reaction termination, measurements, and IC_{50} determinations were performed in the same way as for Pim-1.

Cell cycle analysis: Cell cycle analysis was performed after treatment with kinase inhibitors (**Ru**, 1 and 3 μM, for 24 h or **Os**, 1 and 3 μM for 24 h). 1–2 × 10^6 cells were grown adherently on a culture dish, and were then harvested, washed in cold PBS, and resuspended in cold PBS (200 μL). Cells were fixed by adding the above-mentioned cell solution (200 μL) to 70% ethanol (4 mL), and were incubated on ice for at least 1 h. Intracellular DNA was labeled with a propidium iodide solution (200 μL) that contained 40 μg mL^{-1} propidium iodide and 100 μg mL^{-1} RNase in PBS, and was then incubated at 37 °C for 30 min in darkness. Samples were analyzed by using an EPICS XL (Beckman–Coulter, Inc., Miami, FL). The cell cycle profile was obtained by analyzing 15000 cells. Data were analyzed by using WinMDI software, and apoptosis was defined by the percentage of cells in the sub-G1 fraction of the cell cycle.

Cytotoxicity measurements in 1205 Lu cell culture: 1205 Lu melanoma cells were maintained in DMEM medium plus 2% fetal bovine serum (FBS) at 37 °C under an atmosphere of 5% CO_2 at constant humidity. For each experiment, cells were plated into a 96-well plate with 2500–3000 cells/well and left to grow for 24 h. Thereafter, cells were treated with increasing concentrations of **Os** and **Ru** and 1% DMSO (which is a consequence of the DMSO inhibitor stock solution) for 72 h. As a control, the same number of cells was treated with 1% DMSO. After the treatment, a solution of 3-(4,5-dimethylthiazol-2-yl)-2,5-diphenyltetrazolium bromide (MTT, 5 mg mL^{-1}, 20 μL) in PBS was added to each well. Cells were incubated with MTT for 3 h, and after which time, the media was removed. This was followed by the addition of DMSO (100 μL) to solubilize the resulting purple crystals. Absorbance of each well was measured at 540 nm in a plate reader, and the cell survival in the presence of inhibitors was calculated as a percentage of control absorbance. Experiments were repeated five times and the average value was taken.

Cytotoxicity measurements in 1205 Lu spheroids: Melanoma spheroids were prepared by using the liquid overlay method. Briefly, melanoma cells (200 μL; 25000 cells per mL) were added to a 96-well plate that was coated with 1.5% agar (Difco, Sparks, MD). Plates were left to incubate for 72 h, by which time cells had organized into 3D spheroids. The spheroids were then harvested by using a P1000 pipette. The media was removed and the spheroids were implanted into a gel of bovine collagen I that contained EMEM, L-glutamine, and 2% FBS. Normal 2% melanoma media was overlayed on top of the solidified collagen. Spheroids were treated with either **Ru** (1–3 μM) or **Os** (1–3 μM), before being left to grow for 72 h. Spheroids were then washed twice in PBS before being treated with calcein-AM and ethidium bromide (Molecular Probes,

Eugene, OR) for 1 h at 37 °C, according to the manufacturers instructions. After this time, pictures of the invading spheroids were taken by using a Nikon-300 inverted fluorescence microscope.

Wnt activation in cell culture: OT Luc cells, kindly provided by Dr. Peter Klein (University of Pennsylvania, USA), were maintained in DMEM supplemented with 10% fetal bovine serum (FBS) and 1% penicillin/streptomycin at 37 °C under an atmosphere that contained 5% CO_2 at constant humidity. Cells were plated on 6-well plates (250000 cells/well in 2 mL of medium) and allowed to attach for 24 h. Thereafter, the medium was exchanged with fresh medium (2 mL) and inhibitors were added (10 μL, 200× concentrated in 100% DMSO). After incubation with different concentrations of inhibitor for 24 h, cells were washed with cold PBS (1 mL). The luciferase assay system (Promega) was used for cells lysis and the luciferase assay. Accordingly, cells were harvested and lysed with lysis buffer (200 μL) supplemented with protease inhibitor cocktail and phosphatase inhibitor cocktails I and II from Sigma. The lysates were transferred into 1.5 mL tubes, vortexed for 10 sec, and left on ice for 30 min to ensure complete lysis. Cells were spun down at 10000 rpm at 4 °C for 20 min. Supernatants were stored at −80 °C until luminescence measurements. For luminescence measurements, luciferase substrate was dissolved in assay buffer according to the manufacturers protocol (5 μL of lysate was added into 100 μL of substrate) and luminescence signals were measured immediately with a Monolight 3010 Luminometer from BD Biosciences.

Acknowledgements

E.M. gratefully acknowledges support for this work from the US National Institutes of Health (GM071695), the Camille and Henry Dreyfus Foundation, and the Alfred P. Sloan Foundation (BR-4634). We thank Dr. J.É. Debreczeni and Dr. L. Di Costanzo for their initial assistance with refining the Pim-1 structure. J.M. and D.S.W. contributed equally to this work.

[1] Metal-based drugs: a) C. Orvig, M. J. Abrams, *Chem. Rev.* **1999**, *99*, 2201–2842; b) Z. Guo, P. J. Sadler, *Angew. Chem.* **1999**, *111*, 1610–1630; *Angew. Chem. Int. Ed.* **1999**, *38*, 1512–1531; c) N. Farrell, *Coord. Chem. Rev.* **2002**, *232*, 1–230; d) D. Schlawe, A. Majdalani, J. Velcicky, E. Heßler, T. Wieder, A. Prokop, H.-G. Schmalz, *Angew. Chem.* **2004**, *116*, 1763–1766; *Angew. Chem. Int. Ed.* **2004**, *43*, 1731–1734; e) P. J. Dyson, G. Sava, *Dalton Trans.* **2006**, 1929–1933; f) U. Schatzschneider, N. Metzler-Nolte, *Angew. Chem.* **2006**, *118*, 1534–1537; *Angew. Chem. Int. Ed.* **2006**, *45*, 1504–1507; g) W. H. Ang, P. J. Dyson, *Eur. J. Inorg. Chem.* **2006**, 4003–4018.

[2] a) D. Wang, S. J. Lippard, *Nat. Rev. Drug Discovery* **2005**, *4*, 307–320; b) L. Kelland, *Nat. Rev. Cancer* **2007**, *7*, 573–584.

[3] Y. K. Yan, M. Melchart, A. Habtemariam, P. J. Sadler, *Chem. Commun.* **2005**, 4764–4776.

[4] E. Hillard, A. Vessières, L. Thouin, G. Jaouen, C. Amatore, *Angew. Chem.* **2006**, *118*, 291–296; *Angew. Chem. Int. Ed.* **2006**, *45*, 285–290.

[5] a) A. F. A. Peacock, A. Habtemariam, S. A. Moggach, A. Prescimone, S. Parsons, P. J. Sadler, *Inorg. Chem.* **2007**, *46*, 4049–4059; b) A. F. A. Peacock, A. Habtemariam, R. Fernández, V. Walland, F. P. A. Fabbiani, S. Parsons, R. E. Aird, D. I. Jodrell, P. J. Sadler, *J. Am. Chem. Soc.* **2006**, *128*, 1739–1748.

[6] P. Pigeon, S. Top, A. Vessières, M. Huché, E. A. Hillard, E. Salomon, G. Jaouen, *J. Med. Chem.* **2005**, *48*, 2814–2821.

[7] H. Bregman, D. S. Williams, G. E. Atilla, P. J. Carroll, E. Meggers, *J. Am. Chem. Soc.* **2004**, *126*, 13594–13595.

[8] D. S. Williams, G. E. Atilla, H. Bregman, A. Arzoumanian, P. S. Klein, E. Meggers, *Angew. Chem.* **2005**, *117*, 2020–2023; *Angew. Chem. Int. Ed.* **2005**, *44*, 1984–1987.

[9] G. E. Atilla-Gockumen, D. S. Williams, H. Bregman, N. Pagano, E. Meggers, *ChemBioChem* **2006**, *7*, 1443–1450.

[10] J. É Debreczeni, A. N. Bullock, G. E. Atilla, D. S. Williams, H. Bregman, S. Knapp, E. Meggers, *Angew. Chem.* **2006**, *118*, 1610–1615; *Angew. Chem. Int. Ed.* **2006**, *45*, 1580–1585.

[11] E. Meggers, G. E. Atilla-Gokcumen, H. Bregman, J. Maksimoska, S. P. Mulcahy, N. Pagano, D. S. Williams, *Synlett* **2007**, *8*, 1177–1189.

[12] K. S. M. Smalley, R. Contractor, N. K. Haass, A. N. Kulp, G. E. Atilla-Gokcumen, D. S. Williams, H. Bregman, K. T. Flaherty, M. S. Soengas, E. Meggers, M. Herlyn, *Cancer Res.* **2007**, *67*, 209–217.

[13] a) A. F. A. Peacock, S. Parsons, P. J. Sadler, *J. Am. Chem. Soc.* **2007**, *129*, 3348–3357; b) A. Dorcier, W. H. Ang, S. Bolano, L. Gonsalvi, L. Juillerat-Jeannerat, G. Laurenczy, M. Peruzzini, A. D. Phillips, F. Zanobini, P. J. Dyson, *Organometallics* **2006**, *25*, 4090–4096; c) A. F. A. Peacock, M. Melchart, R. J. Deeth, A. Habtemariam, S. Parsons, P. J. Sadler, *Chem. Eur. J.* **2007**, *13*, 2601–2613; d) B. Cebrián-Losantos, A. A. Krokhin, I. N. Stepanenko, R. Eichinger, M. A. Jakupec, V. B. Arion, B. K. Keppler, *Inorg. Chem.* **2007**, *46*, 5023–5033.

[14] Structural comparison of homologous complexes of osmium and ruthenium: a) U. A. Gregory, S. D. Ibekwe, B. T. Kilbourn, D. R. Russell, *J. Chem. Soc. A* **1971**, 1118–1125; b) H. W. Roesky, K. K. Pandey, W. Clegg, M. Noltemeyer, G. M. Sheldrick, *Dalton Trans.* **1984**, *4*, 719–721; c) M. O. Albers, D. C. Liles, D. J. Robinson, A. Shaver, E. Singleton, M. B. Wiege, J. C. A. Boeyens, D. C. Levendis, *Organometallics* **1986**, *5*, 2321–2327; d) F. A. Cotton, M. P. Diebold, M. Matusz, *Polyhedron* **1987**, *6*, 1131–1134; e) C.-C. Cheng, J. G. Goll, G. A. Neyhart, T. W. Welch, P. Singh, H. H. Thorp, *J. Am. Chem. Soc.* **1995**, *117*, 2970–2980; f) D. Sellmann, M. W. Wemple, W. Donaubauer, F. W. Heinemann, *Inorg. Chem.* **1997**, *36*, 1397–1402; g) R. D. Adams, U. Bunz, B. Captain, W. Fu, W. Steffen, *J. Organomet. Chem.* **2000**, *614–615*, 75–82; h) H. Sugimoto, C. Matsunami, C. Koshi, M. Yamasaki, K. Umakoshi, Y. Sasaki, *Bull. Chem. Soc. Jpn.* **2001**, *74*, 2091–2099; i) S. Baitalik, U. Florke, K. Nag, *Inorg. Chim. Acta* **2002**, *337*, 439–449; j) J. A. Cabeza, I. del Rio, V. Riera, M. Suarez, C. Alvarez-Rua, S. Garcia-Granda, S. H. Chuang, J. R. Hwu, Eur. *J. Inorg. Chem.* **2003**, 4159–4165; k) M. Finze, E. Bernhardt, H. Willner, C. W. Lehmann, F. Aubke, *Inorg. Chem.* **2005**, *44*, 4206–4214.

[15] Comparison of the kinetic inertness of ruthenium and osmium complexes: a) D. T. Richens, *The Chemistry of Aqua Ions*, Wiley, Chichester, **1997**, pp. 421–429; b) W. P. Griffith, *Comprehensive Coordination Chemistry* (Ed.: G. Wilkinson), *Vol. 4*, Pergamon, Oxford, **1987**, Chapter 46, pp. 519–633; c) P. A. Lay, W. D. Harman, *Adv. Inorg. Chem.* **1991**, *37*, 219–379; d) J. Halpern, L. Cai, P. J. Desrosiers, Z. Lin, *Dalton Trans.* **1991**, 717–723; e) R. George, J. M. Andersen, J. R. Moss, *J. Organomet. Chem.* **1995**, *505*, 131–133.

[16] a) H. Bregman, D. S. Williams, E. Meggers, *Synthesis* **2005**, 1521–1527; b) N. Pagano, J. Maksimoska, H. Bregman, D. S. Williams, R. D. Webster, F. Xue, E. Meggers, *Org. Biomol. Chem.* **2007**, *5*, 1218–1227.

[17] a) D. A. Freedman, T. P. Gill, A. M. Blough, R. S. Koefod, K. R. Mann, *Inorg. Chem.* **1997**, *36*, 95–102; b) F. P. Dwyer, J. W. Hogarth, R. N. Rhoda, *Inorg. Synth.* **1957**, *5*, 206–207.

[18] A slight difference in the polarity of **Ru** and **Os** might account for these differences in the binding affinity to GSK-3. To compare the molecular polarities of **Os** and **Ru**, we co-injected a mixture of **Ru** and **Os** onto a Varian Microsorb MV 100–5 Si HPLC column (250× 4.6 mm), which was eluted with EtOH/Hexanes 1:3 at a flow rate of 1 mL min^{-1}. The retention time for **Os** was 11.1 min relative to 11.8 min for **Ru**; this indicates a slightly higher hydrophobicity of **Os** over **Ru**.

[19] a) P. Cohen, S. Frame, *Nat. Rev. Mol. Cell Biol.* **2001**, *2*, 769–776; b) R. S. Jope, G. V. W. Johnson, *Trends Biochem. Sci.* **2004**, *29*, 95–102.

[20] F. Zhang, C. J. Phiel, L. Spece, N. Gurvich, P. S. Klein, *J. Biol. Chem.* **2003**, *278*, 33067–33077.

[21] It is noteworthy that altering the structure of **Ru** by replacing the imide nitrogen for a methyl group abolishes the bioactivity almost completely. For example, this methylated derivative does not affect cell growth and survival at all, even at concentrations as high as

3 μM. This again illustrates that it is not the metal itself that is responsible for the bioactivity but clearly the overall structure of the organometallic complex.
[22] A. N. Bullock, J. É. Debreczeni, O. Y. Fedorov, A. Nelson, B. D. Marsden, S. Knapp, *J. Med. Chem.* **2005**, *48*, 7604–7614.
[23] Z. Otwinowski, W. Minor, *Methods Enzymol.* **1997**, *276*, 307–326.
[24] J. Navaza, *Acta Crystallogr. Sect. A* **1994**, *50*, 157–163.
[25] G. N. Murshudov, A. A. Vagin, E. J. Dodson, *Acta Crystallogr. Sect. D* **1997**, *53*, 240–255.
[26] T. A. Jones, J.-Y. Zou, S. W. Cowan, M. Kjeldgaard, *Acta Crystallogr. Sect. A* **1991**, *47*, 110–119.

Received: February 17, 2008
Published online: April 18, 2008

